COLO–HEP–350

December 1994

Studies of tau decay modes with K^0 mesons from CLEO

J. G. Smith *

Department of Physics, University of Colorado
Boulder, Colorado 80309-0390

We examine five final states involving K^0 mesons, presenting branching fractions for the decays $\tau \to K^0\pi\nu_\tau$, $\tau \to K^0\pi\pi^0\nu_\tau$, $\tau \to K^0K\nu_\tau$, $\tau \to K^0K\pi^0\nu_\tau$, and $\tau \to K_SK_Sh\nu_\tau$. The mass spectra provide evidence for the dominant role of K^* in $K\pi$ decays and K_1 in $K\pi\pi$ modes. We find evidence for a significant K^*K contribution to the $KK\pi$ decays.

1. INTRODUCTION

Although tau decays to final states with kaons were first seen more than ten years ago, only quite recently have experiments had sufficiently large data samples to measure the branching fraction with any precision or attempt detailed studies of the decay dynamics. There are many interesting issues: tests of Cabibbo suppression; SU(3) symmetry breaking [1,2]; and better understanding of the spectral functions and substructure. More precise measurements of kaon modes will allow improved corrections to modes which have been measured without distinguishing between pions and kaons such as $\tau \to h\nu_\tau$, $\tau \to h\pi^0\nu_\tau$, $\tau \to 3h\nu_\tau$, where h signifies a charged π or K. The total branching fraction for modes involving kaons, which amount to a few percent, must be measured well if exclusive decays are to be tabulated accurately [12].

CLEO has published measurements for the decays $\tau \to K\nu_\tau$, $\tau \to K\pi^0\nu_\tau$, and $\tau \to K\pi^0\pi^0\nu_\tau$[3]. Here we present results for the final states K^0h, $K^0h\pi^0$, K^0K, $K^0K\pi^0$, and K_SK_Sh. We present branching fraction measurements, investigate the invariant mass of these states and discuss the implications.

2. EVENT SELECTION

The data included in these analyses was accumulated with the CLEO II detector operating at a center-of-mass energy near 10.6 GeV at the CESR e^+e^- collider. The CLEO detector has been described in detail elsewhere [4]. The integrated luminosity of this sample, 2.96 fb^{-1}, corresponds to 2.7 million produced tau-pair events.

The primary event selection for all measurements is similar. Due to limited space, we will describe the selection for $\tau \to K^0h\nu_\tau$ and $\tau \to K^0h\pi^0\nu_\tau$ and point to any major differences in the other analyses.

A sample of $\tau \to K^0h\nu_\tau$ events is selected by requiring four charged tracks, each with momentum greater than 100 MeV/c and $|\cos\theta| < 0.9$, where θ is the polar angle. We define a 1-3 topology by requiring one track to be isolated, making an angle of at least 90° with each of the other three tracks. If there are any photons in the 1-prong hemisphere with energy greater than 100 MeV, there must be two photons consistent with forming a π^0. A typical event is shown in Fig. 1. To reduce backgrounds from $q\bar{q}$ and 2-photon processes we require that the missing momentum of the event be greater than 300 MeV/c and not point within 32° of the beam direction. The required total energy of the event is between $0.35E_{\mathrm{beam}}$ and $0.8E_{\mathrm{beam}}$. Backgrounds from $q\bar{q}$ events and tau feed-across are reduced by vetoing events which have showers with an energy greater than 100 MeV that are consistent with being photons according to their lateral profile.

The K^0 is identified by requiring two of the tracks in the 3-prong hemisphere to be consistent with the decay $K_S \to \pi^+\pi^-$. The radial flight path of the K_S candidate must be at least 5 mm and

*Work supported by the Department of Energy under grant DE-FG02-91ER40672.

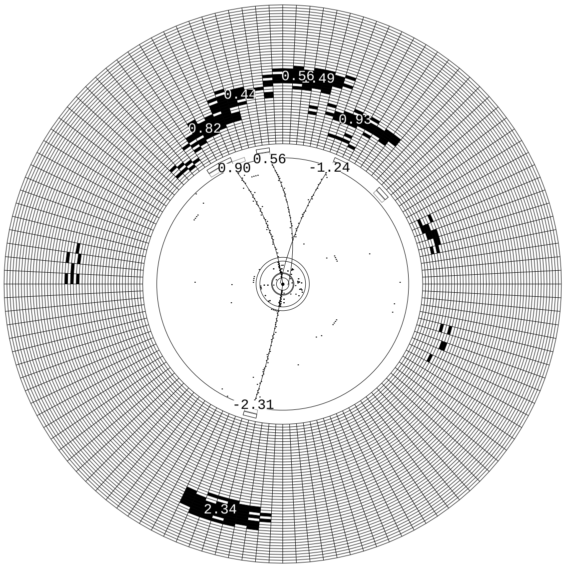

Figure 1. A typical event with a single K_S decay (note detached vertex where tracks intersect). This event is a candidate for a $\tau \rightarrow K^0 h \pi^0 \nu_\tau$ decay, with two nearly-overlapping showers from the $\sim$1 GeV π^0 candidate evident at the top of the figure. The calorimeter is shown in an "exploded" view in which increasing radius is actually increasing z (along the beam direction).

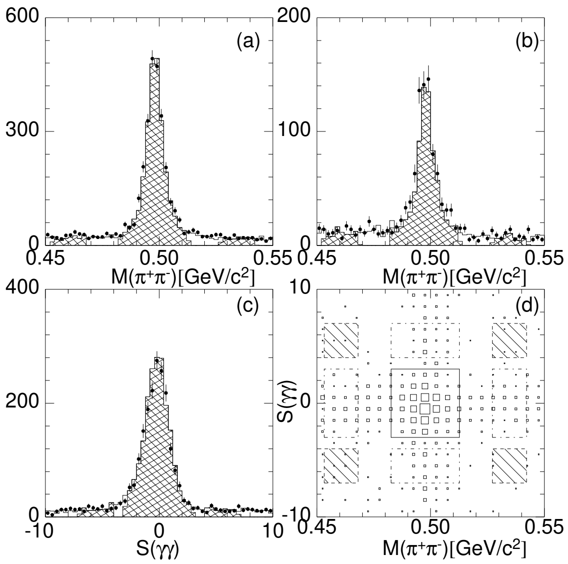

Figure 2. The invariant mass $M_{\pi\pi}$ for $K_S \rightarrow \pi^+\pi^-$ candidates from (a) $\tau \rightarrow K^0 h \nu_\tau$ and (b) $\tau \rightarrow K^0 h \pi^0 \nu_\tau$ candidate events. The points are for the data and the histograms are the MC fractions. For the $\tau \rightarrow K^0 h \pi^0 \nu_\tau$ analysis, we also show (c) the π^0 mass distribution $S_{\gamma\gamma}$ (see text) and (d) $M_{\pi\pi}$ vs $S_{\gamma\gamma}$. The signal and sideband regions are indicated.

the invariant mass of the two tracks, assumed to be pions, must be within 15 MeV of the nominal K_S mass. For the purpose of background subtraction, we define sideband regions which are 37-44.5 MeV above and below the nominal K_S mass. The data and Monte Carlo (MC) mass distributions are shown in Fig. 2(a). The signal and sideband regions are indicated by hatching of the MC histograms. We find 2666 events in the signal region and 359 events in the sideband region. In Fig. 3(a), we show the distribution of the proper time divided by the nominal K_S lifetime, fully corrected for sideband, non-tau and tau feed-across backgrounds (see section 4). The distribution deviates only slightly from an exponential and the MC is in good agreement with the data.

The selection of $\tau \rightarrow K^0 h \pi^0 \nu_\tau$ events proceeds as for $\tau \rightarrow K^0 h \nu_\tau$ events except that a π^0 candidate is required. Such candidates are formed from showers with energy greater than 40 MeV and $|\cos\theta| < 0.71$. The mass of the two pho-

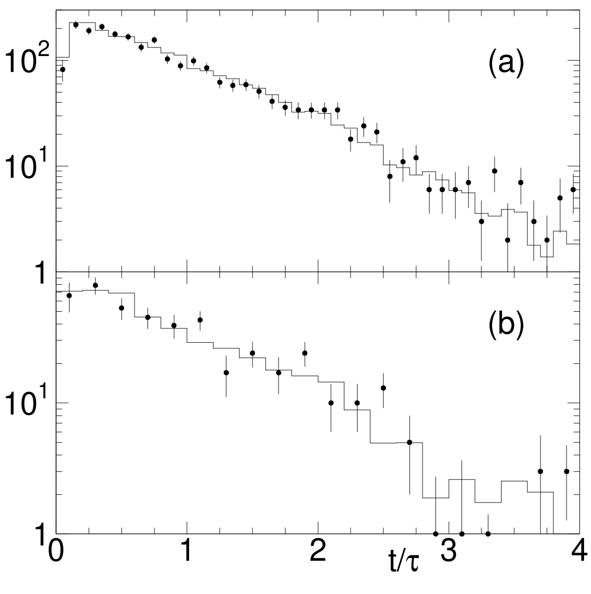

Figure 3. The distribution of t/τ_{K_S} for (a) $\tau \rightarrow K^0 h \nu_\tau$ and (b) $\tau \rightarrow K^0 h \pi^0 \nu_\tau$ candidate events.

tons is required to satisfy $|S_{\gamma\gamma}| < 3$, where $S_{\gamma\gamma} = (M_{\gamma\gamma} - M_{\pi^0})/\sigma_{\gamma\gamma}$. We define sidebands to be 4-7σ from the nominal π^0 mass. The data and MC simulation as well as the signal and sideband regions are shown in Fig. 2. There are 703 (259) events in the signal (sideband) regions. The K_S lifetime distribution for this sample is shown in Fig. 3(b).

Selection of $\tau \to K^0 K(\pi^0)\nu_\tau$ events is similar to that described above. The momentum spectra of the charged kaons (see Fig. 4) is harder than for the pion background modes, suggesting the requirement of a high momentum track. Since the dE/dx information used for K-π separation is ambiguous in the region between 1 and 2 GeV/c, we require the kaon candidate to have a momentum of at least 2.0 GeV/c. Approximately 36% of all $\tau \to K^0 K \nu_\tau$ events and 25% of all $\tau \to K^0 K \pi^0 \nu_\tau$ events pass this cut.

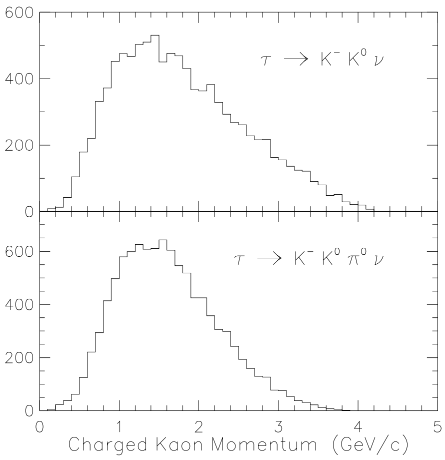

Figure 4. The momentum spectra of charged kaons from (a) $\tau \to K^0 h \nu_\tau$ and (b) $\tau \to K^0 h \pi^0 \nu_\tau$ candidate events.

In order to determine the number of signal events, we choose to fit the normalized dE/dx distribution,

$$\sigma_K \equiv \frac{\frac{dE}{dx}^K_{\rm meas}(p) - \frac{dE}{dx}^K_{\rm exp}(p)}{\sigma_{dE/dx}(p)}, \quad (1)$$

where $\frac{dE}{dx}^K_{\rm meas}(p)$ and $\frac{dE}{dx}^K_{\rm exp}(p)$ are, respectively, the measured and expected specific ionization and $\sigma_{dE/dx}(p)$ is the expected measurement error. The distribution of this quantity for real K's should be a unit-width Gaussian centered at 0. To check that this quantity is being properly described for real K's and π's, we use a calibration sample of $D^* \to D^0 \pi$ decays in which the D^0 decays to $K\pi$. We choose only K or π candidates above 2 GeV/c, to simulate the desired signal momentum range. There is negligible misidentification background for such decays since misidentified events have a D^0 mass which is shifted outside the 3σ mass cut. The sideband-subtracted distribution for $\sim$4000 data events of each type is shown in Fig. 5. The K and π distributions are fit to Gaussians out to $+2\sigma$ and $+3\sigma$, respectively. The means for the K and π peaks are -0.04$\pm$0.02 and 1.63$\pm$0.02, respectively. The standard deviations are 0.99$\pm$0.01 and 1.03$\pm$0.02. For the purposes of fitting the tau data, we fix the means to 0 and 1.63 and the standard deviations to 1.0 and 1.03.

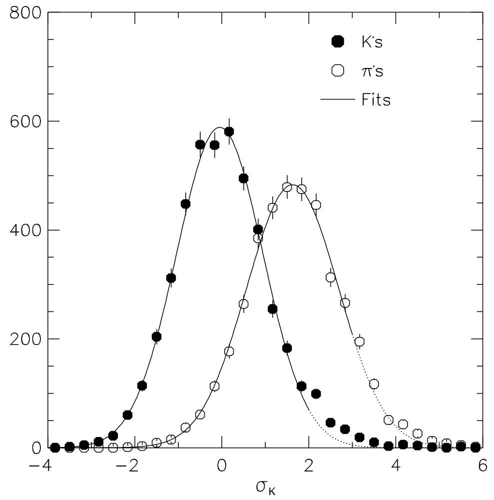

Figure 5. The distribution of σ_K (see eq. (1)) for high-momentum kaons and pions from D^* decays, used for calibrating the σ_K distribution. The fits described in the text are indicated by solid curves.

We extract the number of events in the signal regions by fitting the σ_K distributions of the tau samples. In Fig. 6, we show the 440 data events and fits for the $\tau \to K^0 K \nu_\tau$ sample. The fit yields 142$\pm$17 K's and 288$\pm$21 π's. The latter is in good agreement with the number expected from the known K^* branching fraction. The fit to the number of K's in the K_S sideband samples gives 10.0 ± 4.5 events. Similar fits for the $\tau\to K^0 K\pi^0\nu_\tau$ analysis yield 30 ± 2 events in the signal region (see Fig. 7) and 2 ± 2 events in the sideband region.

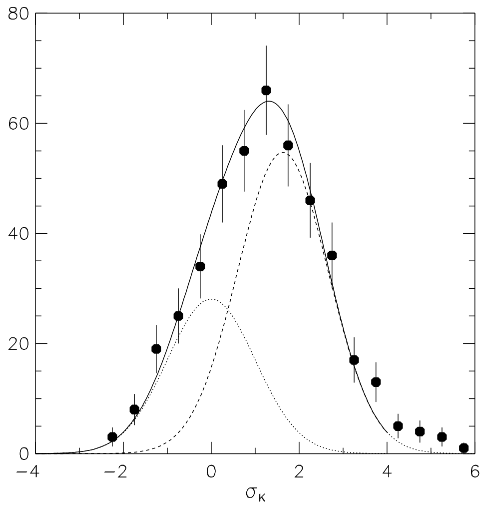

Figure 6. The σ_K distribution for candidate $\tau\to K^0 K\nu_\tau$ events. The data are shown as points with error bars. The dotted and dashed curves indicate the best fit for the kaon and pions components, respectively, and the solid curve indicates their sum.

For the selection of $\tau\to K^0\bar{K}^0 h\nu_\tau$ events we require two K_S candidates satisfying criteria similar to those given above. These criteria are somewhat less restrictive for this analysis in order to keep the selection efficiency as large as possible. The selection results in a sample of 38 events in the signal region and 5 events in the sideband region. In Fig. 8, we show two-dimensional plots of the invariant mass of the two $K_S\to\pi^+\pi^-$ candidates for both data and MC events.

3. MONTE CARLO MODELING

We produce MC samples with appropriate generators and a detailed, GEANT-based [5] detector simulation. We have produced a complete sample of about 8 million tau-pair MC events and other samples for specific signal and background decay modes. We also have generated large samples of

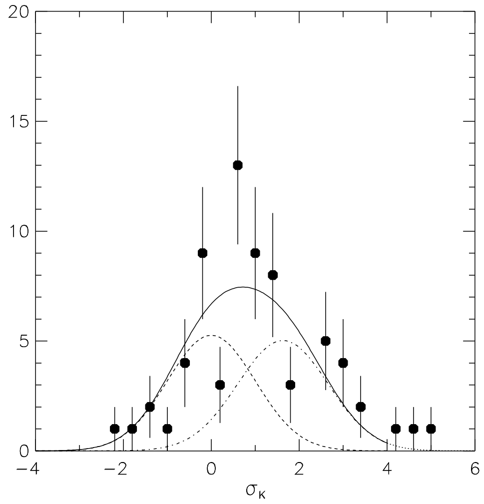

Figure 7. The σ_K distribution for candidate $\tau\to K^0 K\pi^0\nu_\tau$ events. The data are shown as points with error bars and the curves are the same as for the previous figure.

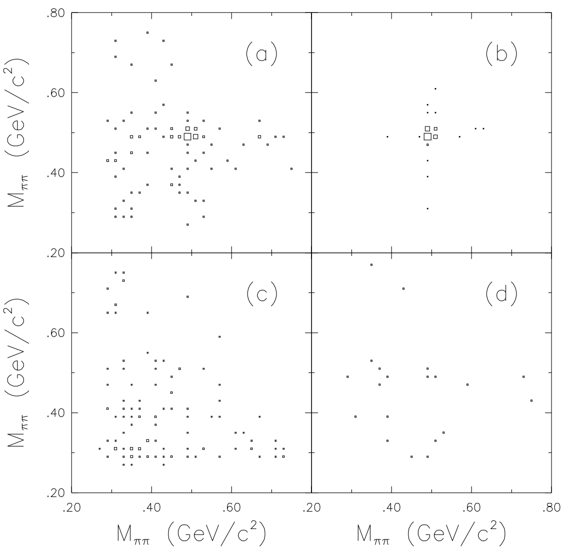

Figure 8. The invariant mass of the two $K_S\to\pi^+\pi^-$ candidates is plotted for (a) data; (b) $K_S K_S h$ signal MC events; (c) tau feed-across background; and (d) $q\bar{q}$ MC.

$q\bar{q}$[6] and $B\bar{B}$ MC to aid in evaluating these backgrounds.

We use the KORALB/TAUOLA package [7] for $e^+e^- \to \tau^+\tau^-$ production and tau decay with several modifications. The situation is quite complex and the dynamics of the simulation are important, so we will describe specifics of the TAUOLA generator in detail. Since the $\tau \to K^0 K \nu_\tau$ decay mode was not included in TAUOLA, we added it, assuming it proceeds via the vector current. We investigate both a flat spectral function model and one in which the $K^0 K$ final state arises from the ρ and ρ'.

The $\tau \to K^0 \pi\pi^0 \nu_\tau$ decay is presumed to proceed through the axial current and the $K_1(1270)$ and $K_1(1400)$ resonances [8,9] though we also consider the possibility of a flat spectral function. We have recently realized that the vector current may also be significant perhaps dominated by the $K^*(1410)$. The contribution of the vector current is negligible in TAUOLA. The possibility of vector-current decays is not considered in the analysis presented in this paper.

The $\tau \to K\bar{K}\pi\nu_\tau$ decay is implemented through contributions from both the vector and axial currents [8] with the former dominated by the ρ' and the latter dominated by the $a_1(1260)$. The relevant decay modes of these resonances are K^*K and $\rho\pi$, where again the ρ decays to $K\bar{K}$. For the a_1 decay, the $\rho\pi$ channel is heavily phase-space suppressed so in the default parameterization of the $\tau \to K^0 \bar{K}^0 \pi \nu_\tau$ decay, $\sim$90% of the decays proceed through K^*K. However for the decay $\tau \to K^0 K \pi^0 \nu_\tau$, there is a cancellation between the two possible K^* charge states causing the axial K^*K contribution to be zero. Since this cancellation may be valid only in the chiral limit, we have modified TAUOLA to include this decay. The default TAUOLA also has no vector contribution to the decay $\tau \to K^0 K \pi^0 \nu_\tau$ for reasons which are somewhat less clear [10]. We have modified TAUOLA to allow such a vector contribution but do not consider this in the present analysis. For the $\tau \to K^0 \bar{K}^0 \pi \nu_\tau$ decay, TAUOLA has $\sim$70% of the decays going through the axial current and 30% through the vector current. The MC in this case is slightly inaccurate since it treats the two K^0's incoherently while in fact the $K_S K_S \pi$ final state is forbidden through the $\rho\pi$ channel. It is not clear whether this incoherent decay approach is appropriate for the K^*K case.

4. DATA ANALYSIS

For all analyses we determine the branching fraction according to

$$\mathcal{B} = \frac{N_{sig}}{2\sigma_{\tau\tau}\mathcal{L}\epsilon}, \tag{2}$$

where N_{sig} is the number of signal events after sideband subtraction and correction for $q\bar{q}$ and tau-feed-across background, $\sigma_{\tau\tau}$ is the tau-pair production cross section including radiative corrections [7], $\mathcal{L}$ is the integrated luminosity [11], and ϵ is the average efficiency. The efficiency is obtained from the full MC simulation discussed in the previous section, where we are careful to adjust the final MC sample so that there is agreement with the observed mass distributions. As a check, we have also evaluated the branching fraction by integrating over the efficiency-corrected mass distribution. The difference between the two methods is small in all cases and is included in the systematic error estimates. The efficiency ranges from 1.2% for $\tau \to K^0 K \pi^0 \nu_\tau$ to 10% for the $\tau \to K^0 h \nu_\tau$ analysis. The amount of $q\bar{q}$ background varies from $\sim$5% for $Kh(\pi^0)$ to 10-20% for the analyses with two kaons, estimated from the data itself. The amount of tau feed-across background is typically below 10%. The background from $B\bar{B}$ events and 2-photon processes is negligible.

The systematic errors for the five measurements are summarized in Table 1. The total systematic error is determined by summing these uncertainties in quadrature. The branching fractions determined in these five analyses are

$$\begin{aligned}
\mathcal{B}(\tau \to K^0 h \nu_\tau) &= (0.98 \pm 0.02 \pm 0.11)\% &(3)\\
\mathcal{B}(\tau \to K^0 h \pi^0 \nu_\tau) &= (0.52 \pm 0.04 \pm 0.06)\% &(4)\\
\mathcal{B}(\tau \to K^0 K \nu_\tau) &= (0.12 \pm 0.02 \pm 0.02)\% &(5)\\
\mathcal{B}(\tau \to K^0 K \pi^0 \nu_\tau) &= (0.13 \pm 0.05 \pm 0.03)\% &(6)\\
\mathcal{B}(\tau \to K_S K_S h \nu_\tau) &= (.021 \pm .004 \pm .004)\%. &(7)
\end{aligned}$$

We can determine the branching fractions for the modes $\tau \to K^0 \pi(\pi^0)\nu_\tau$ by taking differences (3)−(5) and (4)−(6). Taking into account correlated statistical and systematic errors, we obtain

$$\begin{aligned}
\mathcal{B}(\tau \to K^0 \pi \nu_\tau) &= (0.85 \pm 0.03 \pm 0.11)\% &(8)\\
\mathcal{B}(\tau \to K^0 \pi\pi^0 \nu_\tau) &= (0.39 \pm 0.06 \pm 0.06)\%. &(9)
\end{aligned}$$

If we assume that the $K^0\pi$ state is all K^*(we have not yet performed a fit to prove this point), then we can determine the K^* branching fraction.

Table 1
Summary of systematic uncertainties in %. A $*$ indicates that this uncertainty is included in another row for this analysis.

Source	K^0h	$K^0h\pi^0$	K^0K	$K^0K\pi^0$	$K^0\bar{K}^0h$
Luminosity	1	1	1	1	1
Tau cross section	1	1	1	1	1
Tracking efficiency	5	5	5	5	9
K_S efficiency	5	5	5	5	10
Non-τ backgrounds	3	6	12	20	14
τ backgrounds	5	4	3	0	5
π^0 reconstruction	-	3	-	3	-
Sideband subtraction	3	4	$*$	$*$	$*$
Photon veto	3	3	4	5	-
Tag variation	5	3	-	-	-
Model dependence	$*$	$*$	8	8	2
MC statistics	$*$	$*$	3	3	5
dE/dx uncertainties	-	-	7	7	-
Total	11	12	19	25	21

We use eq. (8) above and the CLEO measurement $\mathcal{B}(\tau\to K^-\pi^0\nu_\tau) = (0.51\pm0.10\pm0.07)\%$ [3] to find

$$\mathcal{B}(\tau\to K^*\nu_\tau) = (1.32 \pm 0.15)\%. \quad (10)$$

Finally in order to determine the branching fraction for the decay $\tau\to K^0\bar{K}^0h\nu_\tau$ from the measured $\tau\to K_SK_Sh\nu_\tau$ rate, we must know whether the K_SK_L final state is suppressed. We would multiply eq. (7) by a factor between two and four, depending on the extent of any suppression of K_SK_L.

5. MASS SPECTRA

The matter of the spectral functions for these decays and the resonant sub-structure is of considerable interest. Since there are two pseudoscalars in the final state, the decay $\tau\to K^0K\nu_\tau$ should proceed through the vector current, though the expectations concerning the spectral function are not clear. In Fig. 9, we show the data with the MC prediction for a flat spectral function and a $\rho\to K\bar{K}$ model superimposed. Each mass bin is derived from a fit to σ_K. Quantitative statements concerning these two possibilities will require further study.

The invariant mass distribution for the K^0h data sample is shown in Fig. 10(a) (the pion mass has been used for h); this plot is sideband subtracted and corrected for tau feed-across and $q\bar{q}$ background. In Fig. 10(b) and (c), we show the

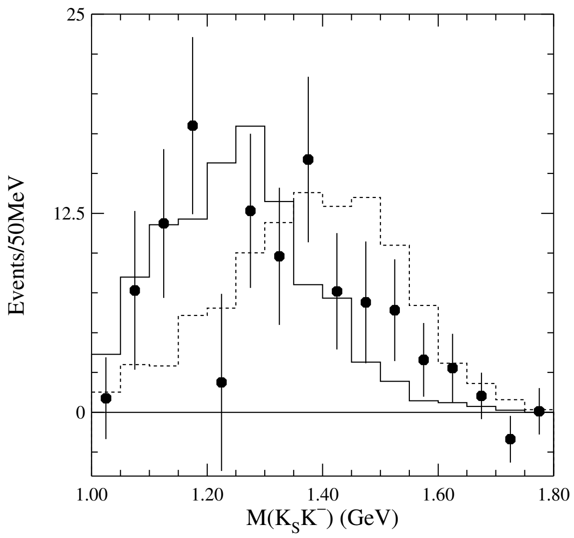

Figure 9. The invariant-mass distribution for $\tau\to K^0K\nu_\tau$ events is shown for data (points), MC for a flat spectral function (dashed histogram), and MC with a $\rho\to K\bar{K}$ model (solid histogram).

MC prediction with hatched contributions from $K_S\pi$ and K_SK, respectively. It is clear that the data are dominated by the $K^*(892)$ resonance, though further analysis is required to quantify this and determine whether there is evidence for non-resonant $K_S\pi$ decays.

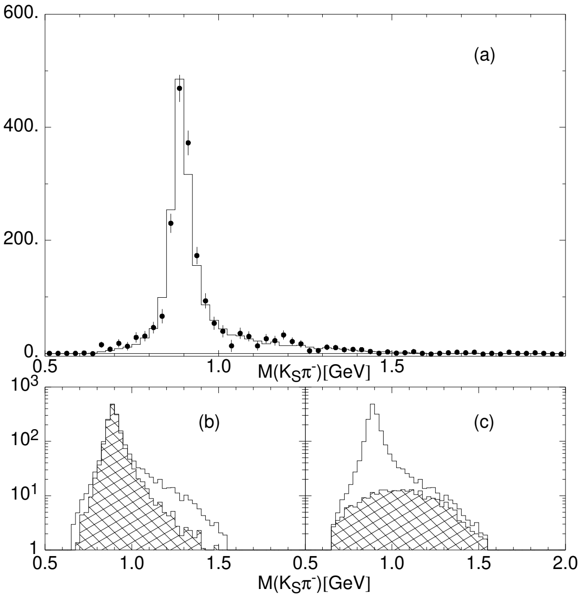

Figure 10. The K^0h invariant-mass distribution for (a) data and MC; (b) MC, $K^*(892)$ hatched; and (c) MC, K_SK hatched from the $\rho\to K^0K$ model. The histogram in (a) and the normalization in (b) and (c) result from a fit to the MC histogram for K^* with the K_SK contribution fixed according to eq. (5).

The situation for the $K^0h\pi^0$ final state is more interesting and much more complicated. As discussed in section 3, this state should have major contributions from $K_1(1270)$, $K_1(1400)$ and $K^0K\pi^0$. We show the invariant mass distribution for data $K_Sh\pi^0$ events in Fig. 11(a), again using m_π for h. In Fig. 11(b), (c) and (d), we show the MC prediction with hatching for $K_1(1270)$, $K_1(1400)$ and $K^0K\pi^0$, respectively. The data are consistent with a K_1 intermediate state with the $K_1(1270)$ contributing substantially more than the $K_1(1400)$. The possible vector contribution from $K^*(1410)$ precludes quantitative conclusions about the amount of $K_1(1400)$ without more detailed study. Such an analysis allowing

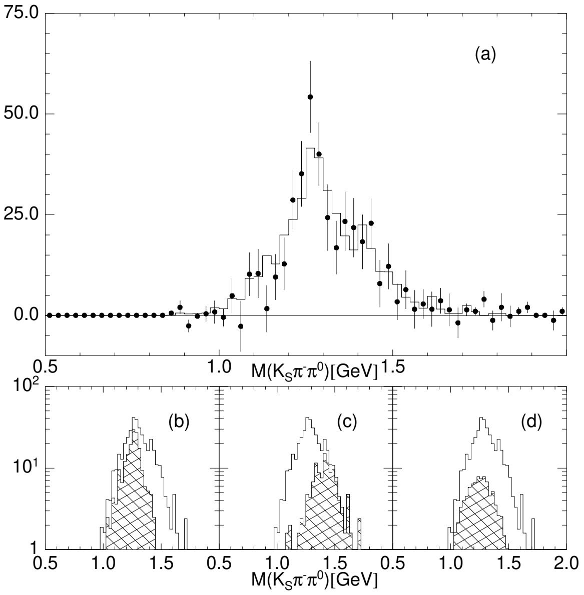

Figure 11. The invariant-mass distribution for $K^0h\pi^0$ events for (a) data with total MC overlaid; (b) MC, $K_1(1270)$ hatched; (c) MC, $K_1(1400)$ hatched; and (d) MC, $K_SK\pi^0$ hatched from the K^*K model. The histogram in (a) and the normalization in (b), (c) and (d) is the result of a fit to the MC predictions for $K_1(1270)$ and $K_1(1400)$ with the $K_SK\pi^0$ contribution fixed according to eq. (6).

interference between the various final states is in progress.

The $K\bar{K}\pi$ final state is also very interesting. We explore this mode in both the $K^0K\pi^0$ and $K^0\bar{K}^0\pi$ final states. In Fig. 12, we show the invariant mass of the $K^0K\pi^0$ system for the data. This and all following plots are sideband subtracted and corrected for tau feed-across background but not $q\bar{q}$ background. Also shown are MC histograms for the axial K^*K and $\rho\pi$ models discussed in section 3. Though the statistical precision is limited, it is clear that the data favor a substantial K^*K contribution, in disagreement with the expectations from the chiral calculations [8]. This is further supported by the fact that the branching fraction (eq. (6)) is comparable to other $K\bar{K}\pi$ charge states [13], as expected from a K^*K intermediate state. In order to investigate the direct evidence for a K^*K intermediate state, we show the $K\pi^0$ invariant masses in Fig. 13. The data cannot distinguish between the K^*K and $\rho\pi$

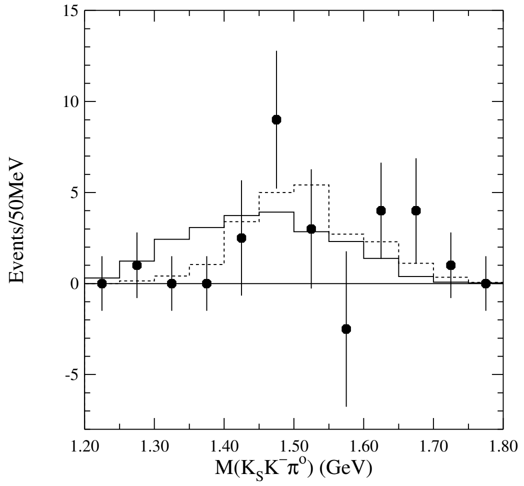

Figure 12. The invariant-mass distribution for $\tau \to K^0 K \pi^0 \nu_\tau$ events is shown for data (points) and axial (a_1) MC. The $K^* K$ and $\rho\pi$ models are shown as solid and dashed histograms, respectively.

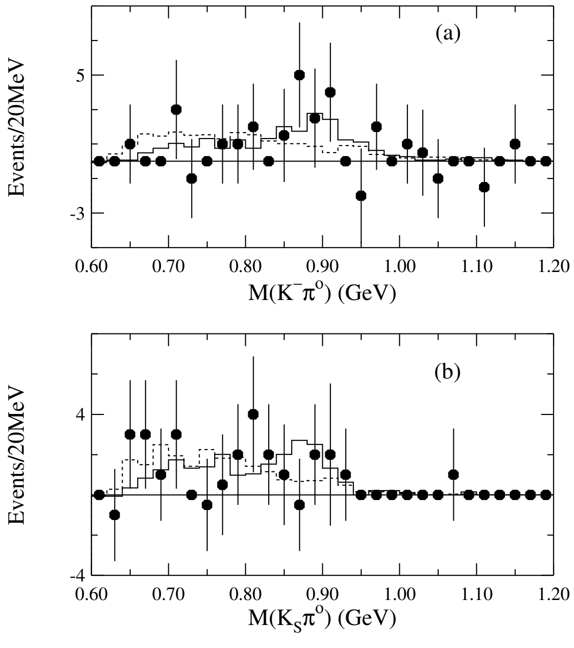

Figure 13. The (a) $K^- \pi^0$ and (b) $K_S \pi^0$ invariant-mass distributions for $\tau \to K^0 K \pi^0 \nu_\tau$ events for data (points) and a_1 MC. The histograms are the same as for the previous figure.

models.

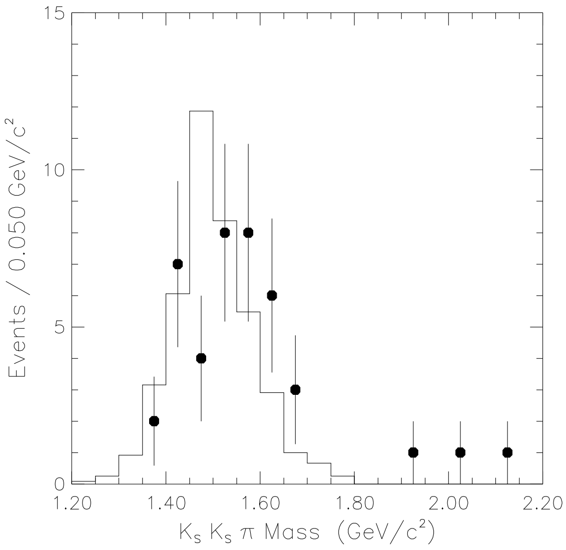

Figure 14. The $K_S K_S \pi$ invariant-mass distribution for $\tau \to K_S K_S h \nu_\tau$ events is shown for data (points) and the MC prediction (histogram).

The mass distribution for the $K_S K_S h$ channel is shown in Fig. 14. Some $q\bar{q}$ background is evident above the tau mass. The MC distribution is also shown, with the parameters as discussed in section 3. The data tend to have a somewhat higher mass than the MC, suggesting that perhaps the vector decay through the ρ' may account for even more than the 30% that is in the MC, though more data are needed. In Fig. 15, we show the $K_S \pi$ invariant mass (two entries per event). A K^* peak is evident, as expected, since the $\rho\pi$ intermediate state is not possible for this decay (see section 3).

6. THEORETICAL COMPARISONS

We have already discussed the theoretical expectations concerning the spectral functions and sub-structure. There are also predictions for the branching fractions given in section 4. Since the mode $\tau \to K^0 K \nu_\tau$ is expected to be dominated by the vector current, in principle it could be extracted from CVC and e^+e^- data. This isn't feasible since the $K\bar{K}$ state in e^+e^- is predominantly isoscalar (due to the ϕ meson). Instead, SU(3)

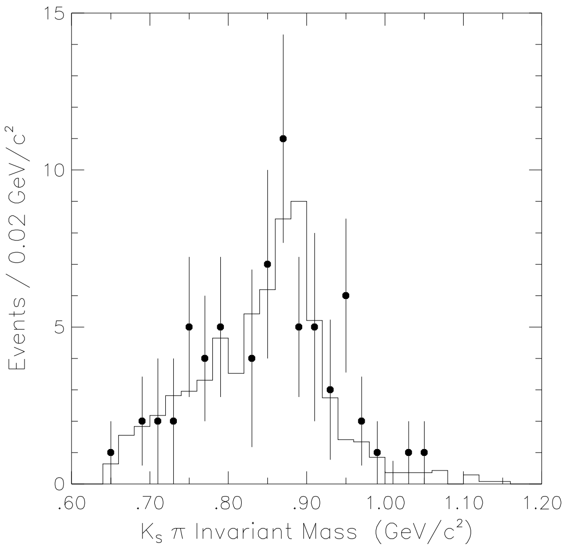

Figure 15. The $K_S\pi^0$ invariant-mass distribution for $\tau \rightarrow K_S K_S h \nu_\tau$ events is shown for data (points) and MC (histogram).

symmetry is used to relate $K\bar{K}$ to $\pi\pi$, with the prediction $\mathcal{B}(\tau \rightarrow K^0 K \nu_\tau)$=(0.12$\pm$0.03)% [15], in excellent agreement with eq. (5).

For the other modes predictions can be derived from the DMO sum rules. The more familiar sum rules [1] relating the strange-current spectral functions were first applied to tau physics by Tsai [14], four years before the discovery of the tau! Marciano [16] has noted more recent work on sum rules by Peccei and Solà [17] and Donoghue and Holstein [18]. The latter paper applies another sum rule [2] to the non-strange, spin-1 currents. This "new" sum rule should be the most reliable since its integrand has an additional power of $1/m^2$, damping contributions from higher-mass resonances. Though it is not mentioned in either Ref. [2] or [18], an SU(3) extension of this sum rule can be used to relate the strange-current spectral functions, similarly to what was done in the original DMO paper [1].

The relevant sum rule relating the strange and non-strange vector currents can be written

$$\int_0^\infty [v(m^2) - v^s(m^2)] dm^2 = 0. \qquad (11)$$

The most naive application of the sum rules uses only a single resonance which dominates each current and a narrow width approximation for each resonance to obtain a relation between tau branching fractions. Such an approach has frequently been used in the past [19] and it leads to the prediction, $\mathcal{B}(\tau \rightarrow K^* \nu_\tau)/\ \mathcal{B}(\tau \rightarrow \rho \nu_\tau)$= $0.93 \tan^2\theta_C = 0.046$ and $\mathcal{B}(\tau \rightarrow K^* \nu_\tau)$=1.15% with the latest world average for $\mathcal{B}(\tau \rightarrow \rho \nu_\tau)$[12]. However, the work of Peccei and Solà shows the importance of the $\tau \rightarrow 4\pi\nu_\tau$ decay in the vector current. Including this contribution increases the prediction for $\mathcal{B}(\tau \rightarrow K^* \nu_\tau)$ to nearly 2%, well above the experimental value. Perhaps this indicates that if one takes radial excitations into account in the vector current (assuming ρ' dominates $\tau \rightarrow 4\pi\nu_\tau$), then one should take them into account in the strange vector current also. The obvious candidate for the latter is the $K^*(1410)$, though this has not yet been seen in tau decays. Alternatively, the sum rule may not work well when cut off at the tau mass.

Other DMO sum rules relate the strange axial current to the strange vector current. Using the single, narrow-resonance approximation, one finds predictions for the total K_1 branching fraction of about 0.4%. This value is comparable to the value from eq. (9); however, when contributions from the other two $K\pi\pi$ charge states are included, the experimental total is about 1% [12]. Further study of this issue without the narrow-width approximation is in progress.

7. CONCLUSIONS

We have reported results for five different tau decays involving K_S mesons. We have measured branching fractions for all these modes with a precision that is better than previous measurements in most cases. The mode $\tau \rightarrow K_S K_S h \nu_\tau$ has not been seen previously. We also have shown invariant-mass distributions for these modes and discussed the theoretical implications of the measurements.

ACKNOWLEDGEMENTS

I would like to thank the organizers, especially Gigi Rolandi and Seamus Hegarty for a wonderful conference. I would especially like to thank Shun Chan, Jay Dominick and Jon Urheim who did all of the actual analysis presented here and provided considerable assistance in the preparation of this paper. I have had a great deal of help from many other CLEO colleagues including Dave Besson, Bill Ford, K.K. Gan, Brian Heltsley, Tomasz Skwarnicki and Alan Weinstein. I also appreciate useful discussions with Roger Decker, Johann Kühn, Bill Marciano, and Erwin Mirkes.

REFERENCES

1. T. Das, V.S. Mathur, and S. Okubo, Phys. Rev. Lett. **18**, 761 (1967).
2. T. Das, V.S. Mathur, and S. Okubo, Phys. Rev. Lett. **19**, 859 (1967).
3. M. Battle *et al.* (CLEO collaboration), Phys. Rev. Lett. **73**, 1079 (1994).
4. Y. Kubota *et al.* (CLEO collaboration), Nucl. Instr. and Meth. Phys. Res., Sect. A **320**, 66 (1992).
5. R. Brun *et al.*, GEANT 3.15, CERN DD/EE/84-1.
6. JETSET 7.3: T. Sjöstrand and M. Bengtsson, Comput. Phys. Commun. **43**, 367 (1987).
7. We use KORALB (v.2.2) / TAUOLA (v.2.4). References for earlier versions are: S. Jadach and Z. Was, Comput. Phys. Commun. **36**, 191 (1985); **64**, 267 (1991); S. Jadach, J. H. Kühn, and Z. Was, Comput. Phys. Commun. **64**, 275 (1991); **70**, 69 (1992); **76**, 361 (1993).
8. R. Decker, E. Mirkes, R. Sauer and Z. Was, Z. Phys. C **58**, 445 (1993).
9. TAUOLA currently includes only the $K_1(1400)$ resonance. We make modifications to allow either $K_1(1270)$ or $K_1(1400)$, but interference between them is absent since both K_1's aren't present.
10. The authors of Ref. [8] state that this is forbidden because "anomalies do not develop second-class currents".
11. G. Crawford *et al.* (CLEO collaboration), Nucl. Instr. and Meth. Phys. Res., Sect. A **345**, 429 (1994).
12. B. Heltsley, presentation at this workshop, CLNS 94/1303.
13. Ref. [12] finds a world average $\mathcal{B}(\tau \rightarrow K^+ K^- \pi \nu_\tau) = (0.20 \pm 0.07)\%$.
14. Y.S. Tsai, Phys. Rev. D **4**, 2821 (1971).
15. S.I. Eidelman, presentation at this workshop; and S.I. Eidelman and V.N. Ivanchenko, Phys. Lett. **B257**, 437 (1991).
16. W.J. Marciano, presentation at this workshop.
17. R. D. Peccei and J. Solà, Nucl. Phys. **B281**, 1 (1987).
18. J.F. Donoghue and B.R. Holstein, Phys. Rev. D **46**, 4076 (1992).
19. B.C. Barish and R. Stroynowski, **The Physics of the τ Lepton**, Physics Reports **157**, 39 (1988).